RESEARCH ARTICLE

Key Points:
- Half of decaying MJO events do so because they encounter westward propagating dry precursors originating in the central Pacific Ocean
- The remainder of decaying events do so because moistening over the southern Maritime Continent is near zero
- ENSO cycles regulate both the frequency of dry precursors and background moisture states that influence MJO propagation and decay

Correspondence to:
C. A. DeMott,
demott@atmos.colostate.edu

Atmospheric Mechanisms for MJO Decay Over the Maritime Continent

Charlotte A. DeMott[1] [ID], **Brandon O. Wolding[1]** [ID], **Eric D. Maloney[1]** [ID], and **David A. Randall[1]**

[1]Department of Atmospheric Science, Colorado State University, Fort Collins,

Abstract Eastward propagating Madden-Julian oscillation (MJO) events that develop in the Indian Ocean from November to April are separated into events whose convective anomalies do and do not propagate across the Maritime Continent (MC). Propagating (P) events are divided into strong (sP) and weak (wP) subsets based on the initial amplitudes of their convective anomalies. Eastward decaying (ED) MJO events have initial amplitudes similar to those of wP events. Roughly half of all MJO events encounter westward propagating transient dry precursor (TDP) signals over the MC. These TDPs, which are external to the MJO circulation system, overwhelm the weak, eastward propagating moist anomaly in ED events, leading to MJO termination. In wP events, the MJO moist anomaly is stronger than the TDP dry anomaly, and the MJO propagates beyond the MC. ED MJO events that do not encounter TDPs decay because of insufficient moistening in the southern MC region. The background states of TDP- and non-TDP-affected MJO events resemble La Niña and El Niño conditions, respectively. The regional regulation of TDP activity and background moisture gradients by El Niño–Southern Oscillation can both be understood in terms of the zonal shift and the meridional expansion or contraction of Warm Pool moisture in response to El Niño–Southern Oscillation sea surface temperature anomalies. Our results demonstrate that modulation of TDPs by the background state moisture can affect the MJO in a manner that reinforces its propagation or decay via the interaction of MJO circulation anomalies and background moisture gradients.

1. Introduction

The Madden-Julian oscillation (MJO) is a large-scale (O[10,000 km]), convectively coupled tropical disturbance that moves eastward at ≈ 5 m/s with a period of 30–70 days (Madden & Julian, 1971, 1972). The MJO convective signal maximizes over the warm waters of the tropical Indian and western Pacific Oceans, but its tropical upper level circulation anomalies can circumnavigate the globe. Equatorial MJO convection weakens as it crosses the MC but reintensifies over the western Pacific Ocean. The observed weakening of MJO equatorial convection within the MC may be linked to a decrease in ocean surface area and evaporative fluxes (Sobel et al., 2010), "siphoning" of intraseasonal energy by the strong diurnal cycle of convection within the MC (Inness & Slingo, 2006), disruption of convective organization by island terrain effects (Hsu & Lee, 2005; Wu & Hsu, 2009), and the detour of convection south of Sumatra and Java during December–February (Kim et al., 2017). As such, the MC may act as a propagation barrier, or hurdle, for MJO convection, but one that is not usually detrimental to the disturbance.

Intense heating from MJO convection excites teleconnection responses that influence a variety of global weather phenomena, including global monsoon systems, atmospheric rivers, cold air outbreaks, heat waves, tornadic activity, sea ice concentrations, significant wave height, the North Atlantic Oscillation, the Southern Annular Mode, and the El Niño–Southern Oscillation (ENSO; Zhang, 2013, and references contained therein). The teleconnection response to the MJO is largest when its convective anomaly traverses the MC and reaches the western Pacific Ocean (e.g., Higgins & Mo, 1997; Matthews & Meredith, 2004). Consequently, skillful simulation of MC-crossing or non-MC-crossing MJO events may improve forecast skill across the globe.

However, an outstanding problem in climate and forecast models is the overprediction of MJO demise before it propagates across the MC (DeMott et al., 2015; Hung et al., 2013; Jiang et al., 2015; Klingaman et al., 2015). This overprediction of MJO decay negatively impacts weather forecast skill because the simulated western Pacific MJO convective heating anomaly that drives extratropical circulation responses is absent or is unrealistically weak (Inness & Slingo, 2006; Neale & Slingo, 2003). Models may struggle with MJO simulation in the vicinity of the MC due to erroneous representations of MC surface fluxes, island-convection interactions,

including spatial- and temporal-scale interactions, and upper ocean responses to MJO forcing (Sobel et al., 2010). More recent studies point to model biases in mean state moisture over the MC as a reason for the overprediction of MJO termination over the MC (Gonzalez & Jiang, 2017; Jiang, 2017; Ling et al., 2017).

Nature provides examples of MJO events that do and do not propagate across the MC. These examples may offer insight into the factors that regulate MJO propagation and can focus efforts to improve its simulation. A plethora of characteristics have been noted for MC-crossing and non-MC-crossing events. For example, MC-crossing MJO events feature anomalous dry conditions to the east of MJO convection (Kim et al., 2014), enhanced eastward and equatorward moisture gradients in the vicinity of the MC (Gonzalez & Jiang, 2017; Kim et al., 2017), and moist preconditioning by low-level horizontal moisture advection (Adames & Wallace, 2015; Kiranmayi & Maloney, 2011; Maloney, 2009, and many others). Non-MC-crossing MJO events exhibit weak or nonexistent dry phases east of MJO convection (Kim et al., 2014), a lack of low-level moistening by horizontal and vertical moisture advection (Hsu & Li, 2012), seasonal and interannual variability (Kerns & Chen, 2016), and a lack of convection over the Indonesian Seas (Zhang & Ling, 2017). Recently, Feng et al. (2015) hypothesized that convection in non-MC-crossing MJO events was disrupted by Rossby wave-like westward propagating midlevel dry anomalies originating in the central Equatorial Pacific. This finding implies that MJO decay over the MC for at least some events is primarily a consequence of dry air propagating into the MC, rather than disruption by processes indigenous to the MC itself.

In this study, we explore the characteristics of MJO events that do and do not propagate across the MC. Because decaying MJO events exhibit weaker initial intensities than the median propagating event, we separate propagating events into initially strong and initially weak categories and focus primarily on differences between decaying and initially weak propagating events. We find that roughly half of all MJO events (both MC- and non-MC-crossing) encounter the westward propagating dry anomalies identified by Feng et al. (2015), and that these interactions can reasonably explain MJO decay for this subset of non-MC-crossing events. Non-MC-crossing MJO events that do not encounter such transient dry anomalies are impeded by zonal and meridional moisture gradients near the MC that hinder moistening by anomalous winds east of MJO convection, as documented in previous studies.

Our paper is organized as follows: Section 2 describes the data and algorithm used for MJO event identification and provides an overview of event characteristics. In section 3, we explore characteristics of westward propagating dry anomalies noted by Feng et al. (2015) that affect some MJO events. Sections 4 and 5, respectively, document the mean state and moistening processes for MJO events that are and are not affected by westward propagating dry anomalies. Our findings are discussed in section 6, and a summary is given in section 7.

2. Methods

2.1. Data

Daily mean outgoing longwave radiation (OLR; Liebmann, 1996) on a 2.5° × 2.5° latitude-longitude grid from 1986 to 2013 is used to identify propagating and nonpropagating MJO events. The beginning date of our analysis period was chosen to include the ocean data record from the Tropical Atmosphere-Ocean (TAO) buoy array (McPhaden et al., 1998) for later analysis of ocean feedbacks.

In this study, we examine MJO propagation from the perspective of moisture theory (e.g., Raymond & Fuchs, 2009), in which MJO propagation is governed by moisture variations. These processes are quantified using the vertically integrated (surface to 100 hPa) moist static energy (MSE) budget (cf. Maloney, 2009) calculated from daily mean fields from the European Centre for Medium Range Weather Prediction Interim Reanalysis (ERA-I; Dee et al. (2011)). MSE is defined as $m = C_p T + gz + Lq$, where C_p is the specific heat of dry air, T is the temperature, g is the gravitational constant, z is the height, L is the latent heat of condensation, and q is the specific humidity. Because MSE is conserved during diabatic processes, its tendency is governed by processes that change the basic state variables, T, z, and q, as follows:

$$\partial \langle m \rangle' / \partial t = -\langle \mathbf{V} \cdot \nabla m \rangle' - \langle \omega \partial m / \partial p \rangle' + \langle LW + SW \rangle' + (LH + SH)' \qquad (1)$$

where brackets denote vertical integration from the surface to 100 hPa, and the terms on the right-hand side of equation (1) represent MSE horizontal advection (HADV), MSE vertical advection, longwave and shortwave radiative heating (LW+SW), and surface latent and sensible heat fluxes (LH+SH). In the tropics, the Coriolis force is weak, and temperature and density perturbations are rapidly dispersed by gravity waves. As a result,
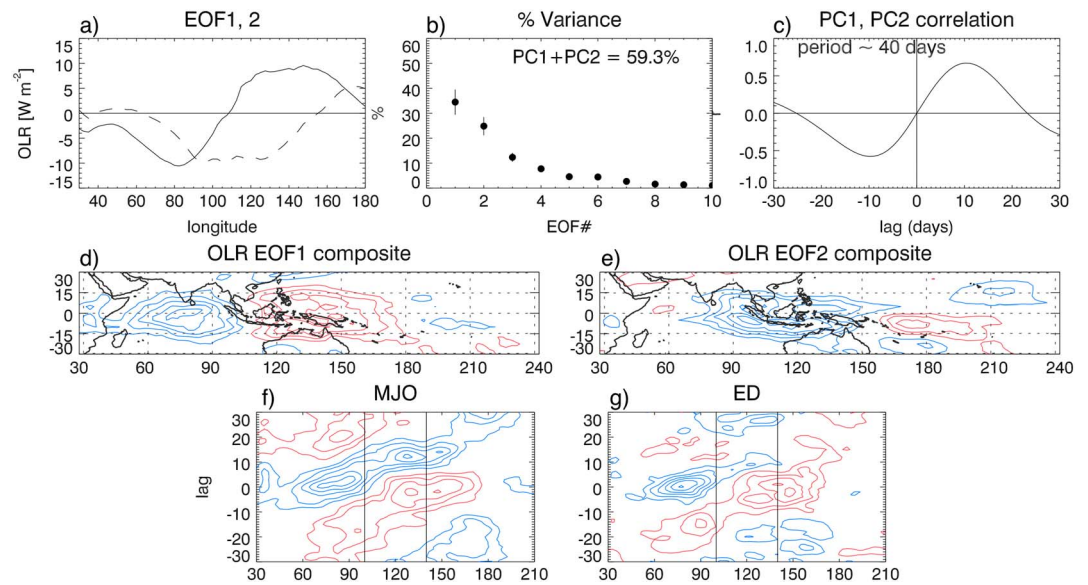
Figure 1. Results from the event selection algorithm: (a) zonal structure of EOF1 (solid) and EOF2 (dashed), (b) fractional variance explained by the first EOFs, (c) lag correlation between PC1 and PC2, spatial loadings of OLR regressed onto (d) PC1 and (e) PC2, and lag-average composites of 10°S–10°N averaged OLR for (f) propagating and (g) decaying MJO events. In Figures 1d–1g, OLR contours are drawn every 5 W/m² with negative (positive) anomalies drawn in blue (red). The zero contour is omitted. EOF = empirical orthogonal function; OLR = outgoing longwave radiation; MJO = Madden-Julian oscillation; ED = eastward decaying; PC = principal component.

tropical MSE perturbations are primarily driven by moisture perturbations. Within the MJO, MSE tendencies are dominated by HADV, (cf. Maloney, 2009), which is dominated by midlevel moisture advection (Adames & Wallace, 2015; DeMott et al., 2014). Some of our analyses, therefore, use specific humidity integrated from 850 to 500 hPa (i.e., $\langle q \rangle_{850-500}$) to interpret MSE HADV.

Daily mean time series of all variables are decomposed into a time-dependent, slowly-varying background state, defined as the 61-day running mean, and departures from this background state. This partitioning retains seasonal and interannual variability in the background state, while intraseasonal and higher-frequency variability are reflected in the anomaly time series.

2.2. MJO Event Criteria and Propagation Characteristics

Propagating events (those whose convective anomaly propagates through the MC) and eastward decaying (ED) MJO events (those whose convective anomaly decays before crossing the MC) are identified using a method similar to that described in Hirata et al. (2013). A 20–100-day bandpass filter is applied to daily mean OLR, which is then averaged from 15°S to 15°N. Next, data from 30°E to 180°E are decomposed into empirical orthogonal functions (EOFs). The two leading EOFs depict MJO convection located over the central Indian Ocean and the Maritime Continent (MC; Figure 1a) and together explain 59.3% of the total variance (Figure 1b). The time-varying principal components (PCs) associated with each EOF are in approximate quadrature and reflect an eastward propagating signal with a mean period of ≈40 days (Figure 1c). Indian Ocean intraseasonal events are identified when November 1 through April 15 temporal maxima in PC1 (cold cloud in the Indian Ocean) exceed one standard deviation (σ). For each Indian Ocean convective event, if a maximum in PC2 (cold cloud over the MC) exceeds 1σ within 20 days after the PC1 maximum, the event is classified as propagating. If no PC2 maximum is observed within this period, or if a PC2 maximum less than 1σ is observed, then the event is classified as ED. The PC2 threshold criteria for propagating events is typically met much sooner than the allowable 20 day window of opportunity, with an average 10 day offset from maximum PC1. The algorithm identified 48 propagating and 17 decaying events.

It is possible that westward propagating or stationary convective perturbations not associated with an MJO will project onto either EOF1 or EOF2. To reduce the likelihood of including such non-MJO events in our composites, two additional criteria are applied. First, we require continuous eastward propagation of at least 30° longitude for the Indian Ocean 10 W/m² OLR anomaly. This requirement rejected five propagating and five decaying events. Second, the 10 W/m² OLR anomaly in propagating events must exhibit continuous
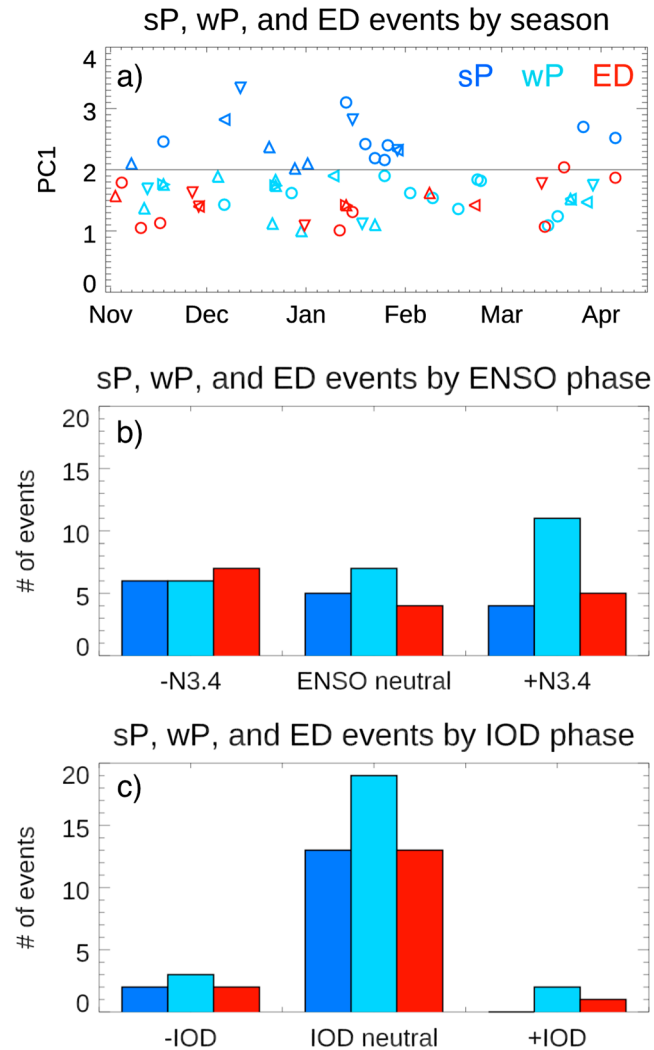
Figure 2. Distribution of sP (dark blue), wP (light blue), and ED (red) MJO events as a function of (a) season, (b) the normalized El Niño–Southern Oscillation (ENSO), as measured by the Niño3.4 index, and (c) the Indian Ocean Dipole moment index. In Figure 2a events developing during ENSO- and IOD-neutral conditions are drawn with circles. Upward- (downward-) pointing triangles indicate events developing during El Niño (La Niña) conditions. Left- (right-) pointing triangles indicate events developing during +IOD (−IOD) conditions. Some events develop during both ENSO and IOD extremes. Horizontal line at PC1 = 2 separates sP and wP events. IOD = Indian Ocean Dipole; MJO = Madden-Julian oscillation; ED = eastward decaying; wP = weak propagating; sP = strong propagating.

propagation from the Indian Ocean to the western Pacific Ocean (gaps less than 10° longitude are allowed). This criteria lead to reassignment of four events from propagating to decaying classifications. These adjustments yielded 39 propagating and 16 ED events.

The seasonal distribution and initial amplitude (as indicated by PC1) of all MJO events is shown in Figure 2a. The initial amplitudes of all but one decaying event are less than 2σ, whereas initial amplitudes of propagating events routinely exceed 2σ. Separating propagating events into initially strong (PC1 $\geq 2\sigma$) and initially weak PC1 $< 2\sigma$ groups enables assessment of MJO initial amplitude on MJO propagation. Hereafter, we refer to each MJO event type as strong propagating (sP), weak propagating (wP), and ED, respectively. Note that "strong" and "weak" refer to the amplitudes of the convectively enhanced and suppressed anomalies in the Indian and western Pacific Oceans (i.e., their projections onto EOF1), respectively, and not to the degree of propagation.

MJO propagation is influenced by low-frequency variability associated with ENSO and the Indian Ocean Dipole (IOD) (Benedict et al., 2015; Pohl & Matthews, 2007; Shinoda, 2005; Wilson et al., 2013; Woolnough et al., 2000). The frequency of sP, wP, and ED events as function of each of these low-frequency modes is shown
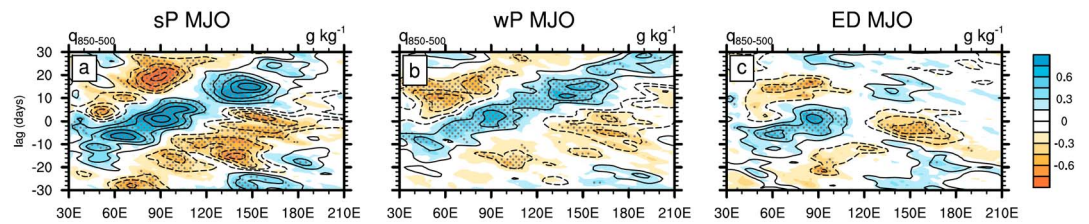
Figure 3. Lagged composites of 15°S–15°N averaged MSE (contours) and $\langle q' \rangle_{850-500}$ (shading) anomalies for (a) sP, (b) wP and (c) ED MJO events. Stippling indicates regions where for $\langle q' \rangle_{850-500}$ averages have less than 5% probability of occurring by chance ($p \leq 0.5$). MSE contour interval is every 2×10^6 J/kg (zero contour omitted), beginning with 2×10^6 J/kg, which corresponds to a probability threshold of $p \leq 0.05$. MSE–$\langle q' \rangle_{850-500}$ correlations for sP, wP, and ED events are $r = 0.88$, 0.87, and 0.85, respectively. sP = strong propagating; wP = weak propagating; ED = eastward decaying.

in Figures 2b and 2c. sP, wP, and ED events are observed during both positive and negative ENSO and IOD phases. wP events, however, are twice as frequent during El Niño than La Niña conditions. As we show later, the El Niño state can improve the chances for wP MJO events to propagate across the MC.

Mean propagation characteristics for each event type are shown with lag averages of 15°S–15°N averaged column-integrated MSE and midlevel moisture anomalies (Figure 3). Here day 0 is the day of maximum OLR projection onto EOF1, which corresponds to maximum convection at about 80°E in the Indian Ocean (Figure 1d). All events exhibit clear eastward propagation in the Indian Ocean. sP and wP events weaken over the MC but reinvigorate in the western Pacific Ocean. ED events, by definition, decay over the MC. The aforementioned relationship between MSE and midlevel moisture is visually apparent.

Propagation characteristics are also assessed using the more traditional real-time multivariate MJO (RMM, Figure 4a) indices (Wheeler & Hendon, 2004) and the OLR MJO Index (OMI, Figure 4b; Kiladis et al., 2014). Day 0 composite RMM amplitudes for each event type are ≈ 1 or greater, although the day 0 RMM amplitude of a few individual events of each type is <1. In these cases, weak projection of the wind anomalies onto the wind components of the RMM index reduces its amplitude (Straub, 2013; Zhang & Ling, 2017). Despite the weak projection of wind anomalies onto the RMM indices in ED events, all three event types exhibit eastward propagation of the MJO signal. The OMI index provides a cleaner comparison of convection amplitude and propagation. Here all but one ED event exceeds $\approx 1\sigma$ of the OMI index (results are not sensitive to inclusion or rejection of this event). Convective signals for all event types exhibit eastward propagation, and the similar initial amplitudes (i.e., the day 0 OMI amplitude) of wP and ED events are evident.

3. Characteristics of Transient Dry Precursors

We refer to the westward propagating dry anomalies identified by Feng et al. (2015) as "transient dry precursors" (TDPs). As previously noted, Feng et al. (2015) suggested that TDPs are dry-phase signatures of Equatorial Rossby (ER) waves. In this section, we summarize the climatology of TDPs, document the frequency with which they encounter MJO convection over the MC, and confirm that their structure and propagation characteristics conform to those of ER waves.

We begin by examining the variability of TDPs over the Warm Pool. Our index for TDP activity is anomalous moisture averaged from 850 to 500 hPa ($\langle q' \rangle_{850-500}$) and then filtered to retain only westward propagating modes. The pressure levels for averaging moisture anomalies were chosen by inspecting longitude-height cross sections in Feng et al. (2015) and are consistent with the height of maximum humidity anomalies for convectively coupled ER waves shown in Kiladis et al. (2009). Spectral analysis of this index for various locations within the Warm Pool (not shown) indicates a broad peak of TDP activity that spans roughly 10–30 days. The November–April variance of this mode is located near 10°N with peaks near 150°E and 80°E (Figure 5a). A secondary band of TDP activity is observed near 15°S. This pattern of activity closely resembles boreal
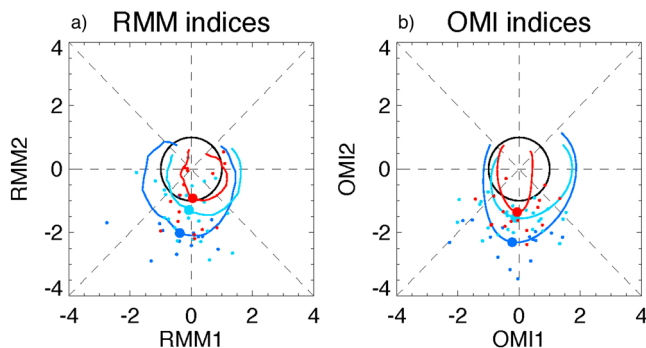

Figure 4. Composite (a) RMM and (b) OMI indices for sP (dark blue), wP (light blue), and ED (red) events from day −15 to day +15. Large dots are the composite day 0 value; small dots are day 0 individual event index values. OMI = OLR MJO index; RMM = real-time Multivariate MJO.
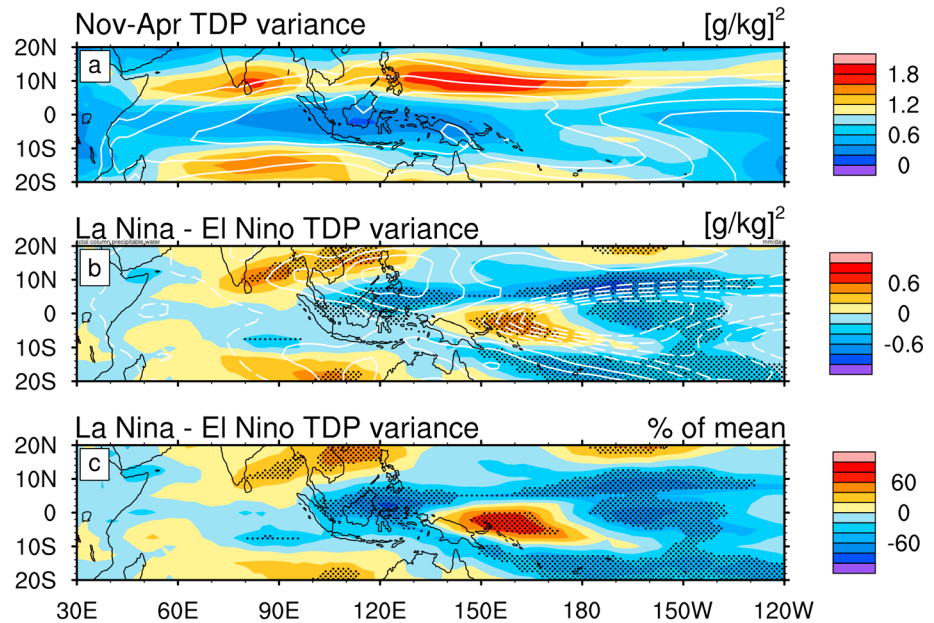
Figure 5. (a) November–April TDP variance (shading) and precipitable water (contours; every 5 kg/m^2 beginning with 40 kg/m^2; (b) as in Figure 5a but for La Niña minus El Niño conditions (contours every 2 kg/m^2; negative values dashed and zero contours omitted); (c) La Niña minus El Niño TDP variance as a percent of the seasonal mean. TDP variance is the 51-day running variance of $\langle q' \rangle_{850-500}$ filtered to retain only westward propagating modes. Stippling denotes significance ($p \leq 0.05$). TDP = transient dry precursor.

winter ER wave activity (e.g., Roundy & Frank, 2004). The bands of maximum TDP activity are the result of sharp meridional moisture gradients near 10°N and 15°S that combine with ER wave meridional wind anomalies to produce strong meridional mixing of moisture. TDP activity is modulated by ENSO cycles (Figures 5b and 5c). In La Niña conditions, TDP activity is suppressed over the western and central MC but enhanced
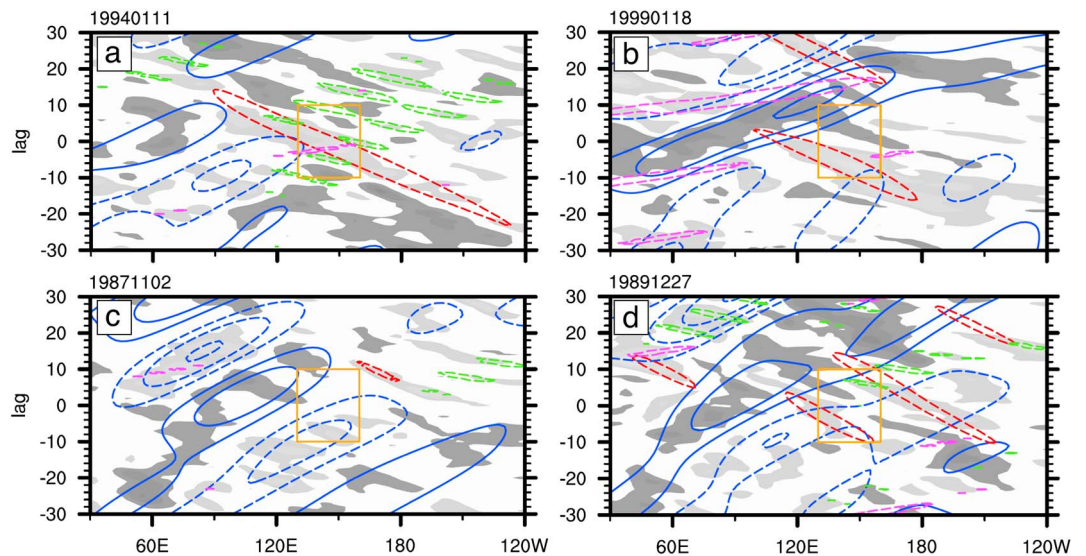
Figure 6. Examples of $\langle q' \rangle_{850-500}$ average 15°S–15°N for MJO events that (a and b) do and (c and d) do not encounter TDPs over the MC. Dark (light) shading is positive (negative) $\langle q' \rangle_{850-500}$ greater than ±0.5 g/kg. MJO (blue), equatorial Rossby wave (ER; red), mixed Rossby-gravity wave (green), and Kelvin wave (magenta) filtered dry anomalies (dashed contours) are overlaid. MJO moist anomalies are solid blue; the zero contour is omitted. Contour interval is 0.25 g/kg for MJO, mixed Rossby-gravity wave, and Kelvin wave, and 0.5 g/kg for ER. Orange square marks longitude-lag boundaries for TDP testing. MC = Maritime Continent; TDPs = transient dry precursors; MJO = Madden-Julian oscillation.

Table 1
MJO Events With and Without Transient Dry Precursors Over the Maritime Continent

Event type	With TDPs	Without TDPs
sP	8	7
wP	8	16
ED	8	8

Note. TDPs = transient dry precursors; ED = eastward decaying; MJO = Madden-Julian oscillation.

over the eastern MC and western Pacific Ocean. In section 5, we hypothesize that the interannual regulation of TDPs may contribute to the successful propagation of initially weak (wP) MJO events across the MC.

To determine how often MJO events are affected by TDPs, we examined each MJO event for TDP activity over the MC. Examples of $\langle q' \rangle_{850-500}$ for ED and wP MJO events are shown in Figure 6. Westward propagating dry anomalies (light shading) associated with ER waves (red) and mixed Rossby-gravity waves (green) are observed at multiple longitudes and lags, indicating that such dry disturbances are not unique to the MC.

In Figures 6a and 6b, the arrival of moist anomalies (dark shading) associated with MJO events (blue contours) coincides with the arrival of a TDP. The TDPs in Figures 6a and 6b originate far from the MJO anomalies and can be regarded as external forcing agents on the MJO environment. In other words, they appear to be separate entities from the shorter-lived, westward propagating dry anomalies contained within the eastward propagating MJO suppressed phase (dashed blue contours) seen in Figures 6c and 6d.

The relative frequency of TDPs influencing the MJO over the MC was assessed using a simple criteria to identify MJO events that do and do not encounter TDPs over the MC. Starting with the 15°S–15°N averaged $\langle q' \rangle_{850-500}$, we identify TDP-affected MJO events by selecting events where westward propagating $\langle q' \rangle_{850-500}$ anomalies ≤ -0.5 g/kg arrive at 160°E between day −10 and day +10. The 0.5 g/kg dry anomaly must then propagate continuously to at least 130°E by day +10. MJO events where the dry anomalies enter the longitude-lag box (shown in orange) but do not meet the propagation requirements, or where the dry anomalies develop within the box are not considered TDP-affected events. Using this criteria, we found that roughly half of all MJO events are affected by TDPs (Table 1). It is worth noting that this criteria only selects MJO-TDP interactions that take place over the MC. Such interactions may also occur throughout the Warm Pool, but we focus on those in the MC region to distinguish MJO decay events whose decay is associated with external influences, such as TDPs, from those whose decay may be governed by processes associated with MC island geography.

A composite TDP for each MJO event type was constructed by regressing assorted variables onto the TDP index (which retains only westward propagating modes) averaged between 140°E–160°E and 10°S–10°N, which roughly corresponds to the region of enhanced TDP activity during MJO events (not shown). Each set of regressions was performed for lags spanning −30 to +30 days. The result for lag day 0 is shown in Figure 7. TDPs interacting with each MJO type exhibit circulation and moisture anomaly patterns typically associated with ER waves (Feng et al., 2015; Kiladis et al., 2009). The dry anomaly (dashed contours in Figure 7) is centered north of the Equator for sP and wP events but on the Equator for ED events.

TDP propagation differences as a function of MJO event are summarized in Figure 8. TDP propagation characteristics are compared to those of ER waves by repeating the regression exercise with ER wave-filtered (westward wave numbers 1–10, period 9–35 days, and equivalent depths 8–90 m) $\langle q' \rangle_{850-500}$ averaged over the same region described above. For sP MJO events (Figure 8a), TDPs appear to originate in the central Pacific Ocean. Their period and propagation speed (4.3 m/s) are similar to those for the convectively coupled ER wave for the same regression base point. In contrast, TDPs that interact with wP and ED MJO events (Figures 8b and 8c) originate in the eastern Pacific Ocean, have a longer period, and propagate more slowly (3.3 m/s and 3.8 m/s, respectively), somewhat slower
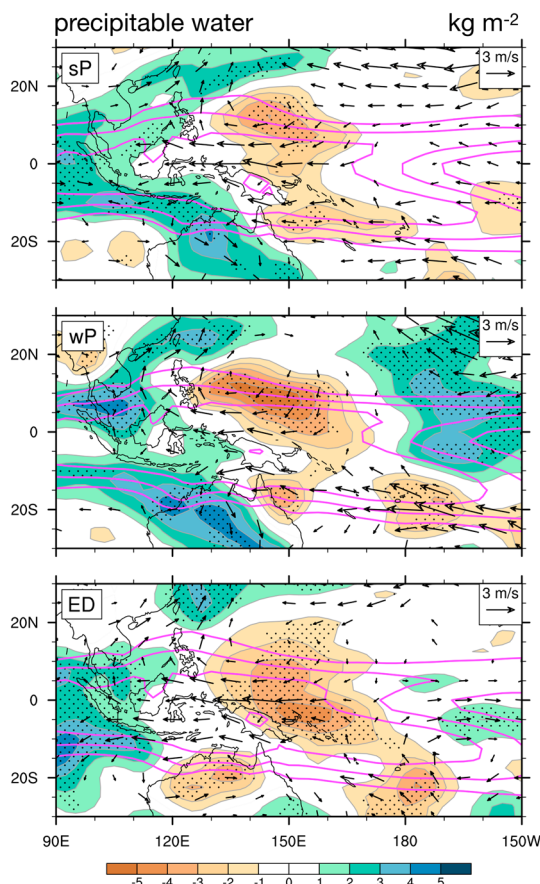
Figure 7. Day 0 composite TDPs for TDP-affected (top) sP, (center) wP, and (bottom) ED MJO events: anomalous precipitable water (shaded; stippling where $p \leq 0.05$); background precipitable water (magenta contours every 5 kg/m² beginning with 40 kg/m²); and 850 hPa wind vectors (drawn if $p \leq 0.05$ for either the zonal or meridional wind). Composites are obtained by regressing anomalous data onto westward propagating $\langle q' \rangle_{850-500}$ averaged from 10°S–10°N and 140°E–160°E. MJO = Madden-Julian oscillation; ED = eastward decaying; sP = strong propagating; wP = weak propagating; TDPs = transient dry precursors.
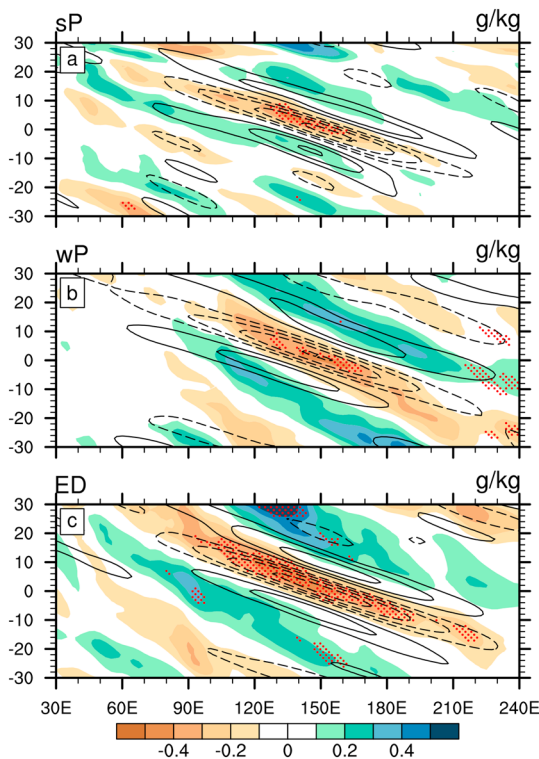
Figure 8. $\langle q' \rangle_{850-500}$ (filtered to retain only westward propagating wave numbers) lag regressed onto its 10°S–10°S and 140°E–160°E area average (shading) for (a) sP, (b) wP, and (c) ED events. Contours show the result for ER wave-filtered (westward wave numbers 1–10, period 9–35 days, and equivalent depths 8–90 m) $\langle q' \rangle_{850-500}$ regressed onto itself averaged over the same region. Contour interval as in the shaded field (negative values dashed and zero contour omitted). ED = eastward decaying; sP = strong propagating; wP = weak propagating; ER = Equatorial Rossby.

than the pure ER wave. The reduction in propagation speed seen in TDPs in wP and ED events may be associated with ER wave interactions with the background three-dimensional wind field. Kiladis and Wheeler (1995) documented such behavior for ER waves, which has been attributed to modulation of ER wave structure by changing background wind states (e.g., Kiladis et al., 2009).
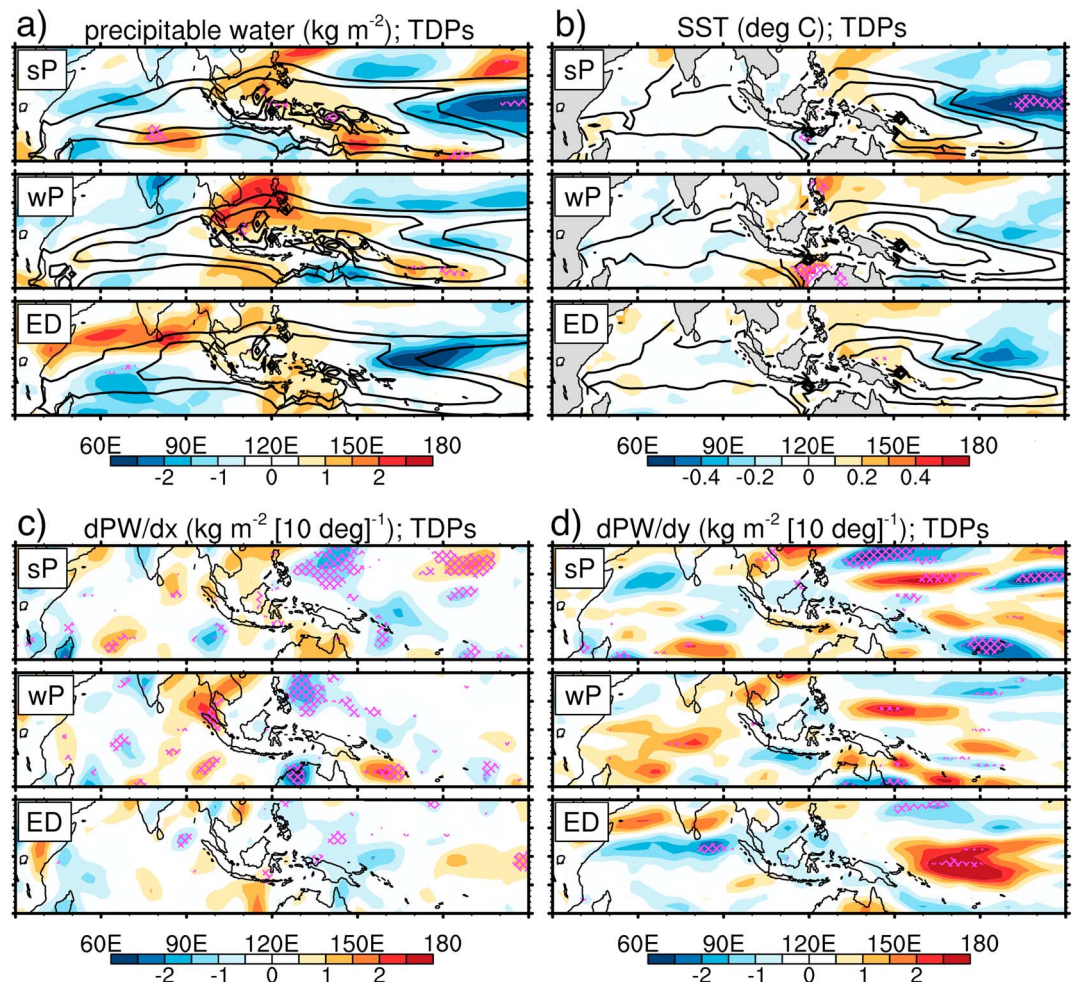
4. MJO Propagation in the Presence of TDPS
4.1. Mean State Conditions for TDP-Affected MJO Events

In this section, we examine only those MJO events that encounter TDPs over the MC. Recent studies have emphasized the importance of the mean state moisture distribution on MJO propagation (e.g., Gonzalez & Jiang, 2017; Kim et al., 2017). The three-dimensional moisture distribution, which is partly tied to the sea surface temperature (SST) distribution, affects convection-moisture feedbacks, including moisture advection by horizontal and vertical winds and cloud-radiation feedbacks. SST plays a role in MJO dynamics via its influence on boundary layer MSE and the overall intensity of convection.

Figures 9a and 9b illustrate mean state precipitable water and SST and their departures from their respective 28-year climatologies. Before computing the mean state, data were filtered to remove 30 to 60-day variability. For an individual event, the mean state is estimated as the 61-day mean of a given variable from −50 days to +10 days. This period enables strict comparison of the background states since it does not include the period when propagation differences appear (after about +10 days). However, we note that the results are essentially the same for a ±30-day averaging period. The anomalous mean state condition for a given event is computed by subtracting the 28-year mean of the same −50 to +10-day period. The composite mean state and its departure from climatology are the average across all events of a given MJO classification (sP, wP, or ED).

Anomalous precipitable water and SST conditions exhibit La Niña characteristics, with cold SST and dry air in the central and eastern Pacific. However, anomalous mean state conditions rarely rise to the level of significance, as indicated by hatching. One notable exception is the region of anomalously warm SSTs in the Northwest Australia Basin in wP events. These warm SSTs help maintain MJO convection via enhanced column moistening by surface fluxes for boreal winter MJO events (DeMott et al., 2016), especially those that primarily "detour" the central MC (Kim et al., 2017).

Zonal and meridional gradients of mean moisture (Figures 9c and 9d, respectively) exhibit regional patterns of enhanced zonal gradients in the eastern Indian Ocean and suppressed zonal gradients in the western Pacific Ocean, consistent with the westward shift of precipitable water. This pattern is most robust for wP events. During the MJO suppressed phase, the enhanced zonal gradients in the Indian Ocean may increase the efficiency of horizontal moisture advection by anomalous low-level easterlies. For meridional moisture gradients (Figure 9d), wP events exhibit enhanced meridional gradients in the Indian Ocean (a few grid points near 70°E are significant), consistent with the more "peaked" or meridionally narrow structure of the Indian Ocean Intertropical Convergence Zone (ITCZ) for wP events (Figure 9a). The sharper meridional gradients in wP events would contribute to more efficient moistening by poleward flow associated with the dry phase of the MJO, in a manner favorable for MJO propagation. In contrast, the more "flat" or meridionally broad structure of the Indian Ocean ITCZ in ED events leads to a northward shift of the meridional gradient and weakened meridional gradients over the Equator. Therefore, Indian Ocean background moisture is less favorable for MJO propagation in ED events.

4.2. Propagation Characteristics of TDP-Affected MJO Events

TDP interactions with the MJO are most apparent when viewed as lagged vertical cross sections of anomalous specific humidity averaged from 10°S to 10°N, as shown in Figure 10 (10°S–10°N was chosen for these cross

Figure 9. Mean state conditions (contours in Figures 9a and 9b) and their departure from climatology (shading) for (a) precipitable water (contours are 45, 50, and 55 kg/m^2), (b) SST (contours are 28.5, 29.0, and 29.5°C), (c) precipitable water zonal gradient, and (d) precipitable water meridional gradient for sP, wP, and ED MJO events affected by TDPs. The mean state is the −50 to +10-day average after 30 to 90-day variability has been removed. Mean state anomalies are departures from the 28-year average of the same 60-day period (see text for explanation). Magenta hatching marks areas where the background state is significantly different from climatology ($p \leq 0.05$). SST = sea surface temperature; TDPs = transient dry precursors; sP = strong propagating; wP = weak propagating; ED = eastward decaying; MJO = Madden-Julian oscillation.

sections to highlight the gradual build up of moisture ahead of MJO convection; this feature is not as apparent for the 15°S – 15°N average used elsewhere in this study). Blue solid lines highlight the MJO moist phase, while red solid lines track the TDP dry anomaly. For sP and wP events, the TDP dry anomaly temporarily merges with the eastward propagating MJO dry anomaly at around day −5 to day 0, where it appears to enhance the MJO dry phase. As the TDP dry anomaly continues its westward progress, it mixes with the MJO moist anomaly. Thus, TDPs may temporarily amplify the MJO dry phase but soon thereafter may erode the MJO moist anomaly.

At day 0, there is a monotonic decrease in the composite MJO moist anomaly from sP to ED events. However, the weakest TDP dry anomaly is observed in the wP event composite. This begs the question of whether TDP-affected ED events decay because the TDP is so dry or because the ED event moist anomaly is not sufficiently moist. To address this question, a comparison of the relative amplitudes of MJO moist anomalies and TDP dry anomalies at day 0 is provided in Table 2. When these two anomalies intersect and mix around day 5, a simple measure of the MJO moisture surplus can be constructed as either the sum or the ratio of the MJO moist and TDP dry anomalies, shown in the bottom two rows of Table 2. By these measures, sP and wP events
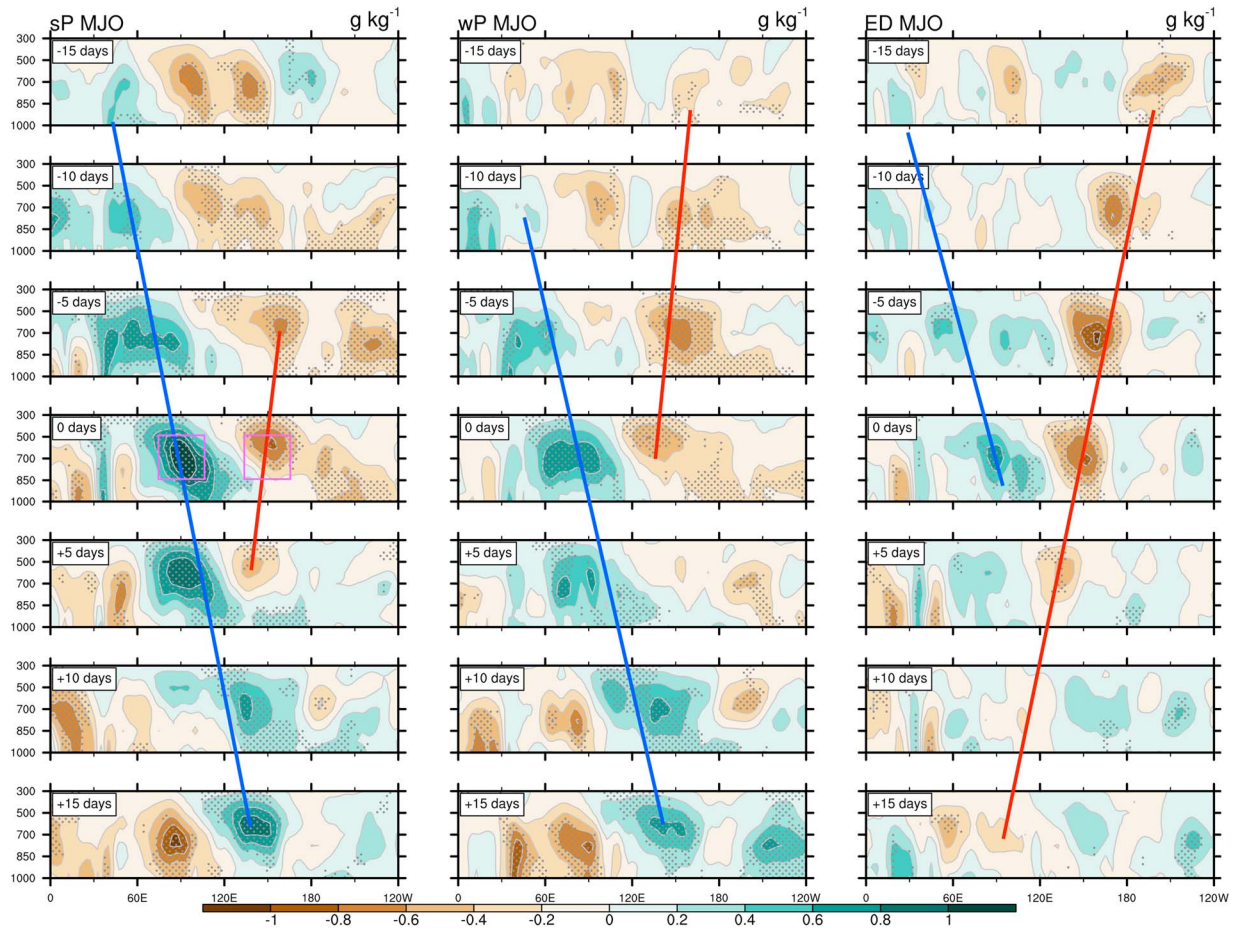
Figure 10. Composite q' longitude-height cross sections averaged 10°S–10°N for TDP-affected sP (right), wP (center), and ED (right) events. Solid blue lines trace MJO moist anomalies. Red solid lines trace TDP moist anomalies. When blue solid and red dashed lines intersect over the MC, TDP dry anomalies reduce MJO moist anomalies. Stippling indicates significance ($p \leq 0.05$). Magenta boxes extend $\pm15°$ longitude about maximum and minimum $\langle q' \rangle_{850-500}$ and illustrate the averaging area for values listed in Table 2. sP = strong propagating; wP = weak propagating; MJO = Madden-Julian oscillation; ED = eastward decaying; TDP = transient dry precursor; MC = Maritime Continent.

have sufficiently large moisture anomalies to withstand mixing with the TDP dry anomaly. The remaining positive moisture anomaly would presumably favor continued convective development and MJO propagation. In contrast, ED events have an MJO moisture deficit, suggesting complete absorption of the MJO moist anomaly and MJO decay. Analysis of standard errors of moist and dry anomalies for each event type (not shown) indicates that the dry anomaly differences are not significant, but the moist anomalies are. This suggests that the amplitude of the MJO moist anomaly is an important factor for MJO propagation in TDP-affected events. The location of the TDP dry anomaly with respect the MC may also affect the extent to which TDPs can interfere with MJO convection. For sP and wP events, the driest air is confined north of the Equator

Table 2
Comparison of MJO Moist and TDP Dry Anomalies by MJO Event Type

	sP	wP	ED
MJO moist anomaly (g/kg)	0.91	0.60	0.44
TDP dry anomaly (g/kg)	−0.50	−0.40	−0.58
moist+dry (g/kg)	0.41	0.20	−0.14
moist/dry	1.81	1.51	0.76

Note. TDP = transient dry precursor; ED = eastward decaying; MJO = Madden-Julian oscillation; sP = strong propagating; wP = weak propagating.
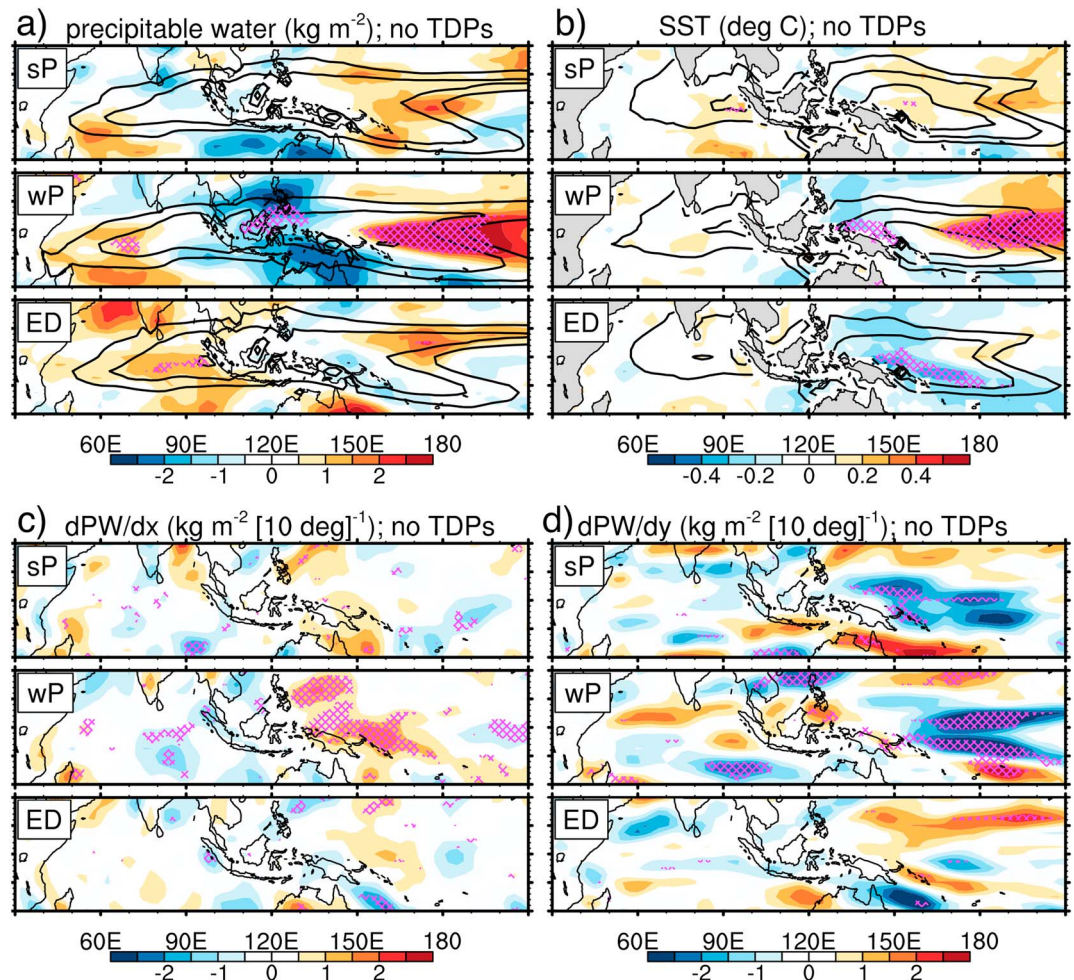
Figure 11. As in Figure 9 but for MJO events not affected by TDPs.

(Figures 7a and 7b), leaving the southern MC relatively unaffected. In contrast, the dry TDP anomaly in ED events spans roughly 10°S–10°N (Figure 7c), increasing the likelihood of mixing with MJO convection.

5. MJO Propagation in the Absence of TDPs

5.1. Mean State Conditions for Non-TDP-Affected MJO Events

In this section, we examine only those MJO events that do not encounter TDPs over the MC. In section 3, we found that TDPs affect MJO convection in roughly half of all ED events (Table 1). This implies that the other half of ED events must decay for other reasons. We again begin with an assessment of the mean state for each class of non-TDP-affected MJO events.

Precipitable water and SST for non-TDP-affected MJO events exhibit characteristics of El Niño conditions, with high precipitable water and warm SSTs near the dateline, and drier conditions and cold SSTs over the MC (Figures 11a and 11b). The El Niño-like condition is most apparent in the wP event composite. For ED events cold SSTs are observed throughout the western Pacific Ocean. For all event types, the eastward shift of precipitable water leads to reduced zonal gradients of moisture in the Indian Ocean, and enhanced zonal gradients in the western Pacific Ocean, especially for sP and wP events (Figure 11c). During the MJO suppressed phase, low-level easterlies and enhanced zonal gradients in the western Pacific Ocean enhance moistening over the MC, which favors MJO propagation.

Anomalous meridional gradients of moisture (Figure 11d) are different for each MJO event type. In sP events, the anomalous meridional gradient is negative everywhere except to the south of the MC and into the South Pacific Convergence Zone (with some areas of significance). The former enhances moistening by MJO
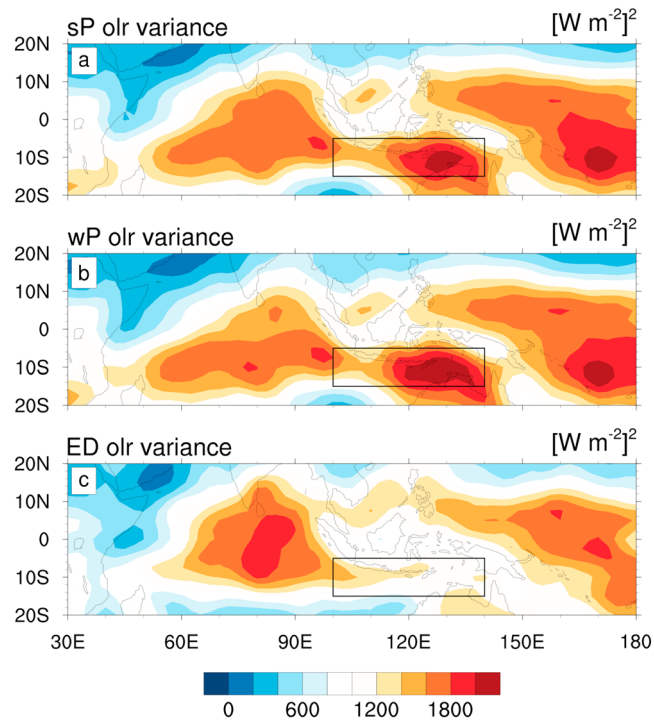
Figure 12. MJO event OLR variance maps for MJO events not affected by TDPs. Results are shown for (a) sP, (b) wP, and (c) ED events. Variance is computed from −30 to +30 days. Boxes mark the "southern MC" averaging area (as defined in Kim et al., 2017) for MSE budget calculations shown in Figure 14. sP = strong propagating; wP = weak propagating; MJO = Madden-Julian oscillation; ED = eastward decaying; TDPs = transient dry precursors; OLR = outgoing longwave radiation; MC = Maritime Continent; MSE = moist static energy.

suppressed phase poleward flow and favors the "detour" of MJO convection to the south of the MC (e.g., Kim et al., 2017). For wP events, meridional gradients are most enhanced within the central MC. Although ED events exhibit modest increases in zonal and meridional moisture gradients in the western Pacific Ocean, the increases are generally not significant. While the same can be said for sP events from about 60°E to 120°E, we now demonstrate that the weaker circulation anomalies in ED events contribute to weak moistening in ED events and their eventual decay.

5.2. Propagation Characteristics of Non-TDP-Affected MJO Events

OLR variance maps (Figure 12) reveal that non-TDP-affected ED events most notably differ from their propagating counterparts over the region just south of the MC. This region is sometimes referred to as the "MC detour region" since it acts as a conduit for MJO convection during December–February (Kim et al., 2017). The evolution of composite OLR and 850-hPa winds is shown in Figure 13 and provides visual context for the southern MC MSE budget analyses that follow. It is interesting to note that convection (blue shading) in wP events is initially weaker than in ED events, but ED events have a weaker and less extensive dry phase (red shading). Despite their similar evolution through day +5, the circulation and convective anomalies in ED events fall apart on day +10.

The vertically integrated MSE budget for the southern MC region for pentads centered on day −5 to day +5 (Figure 14d–f) reveals that the significantly weaker moistening in ED events than in wP events is primarily driven by MSE HADV differences. Although MSE vertical advection and radiative heating also differ significantly for wP and ED events, these column processes almost exactly cancel each other for these event types and cannot explain the difference in total moistening. Zonal advection is the primary reason for the weak moistening in ED events (Figure 14e).

Next, we explore differences in the mean state winds and moisture, as well as their perturbations, to understand the MSE zonal advection differences. Here we use the 850 to 500-hPa averaged moisture budget,
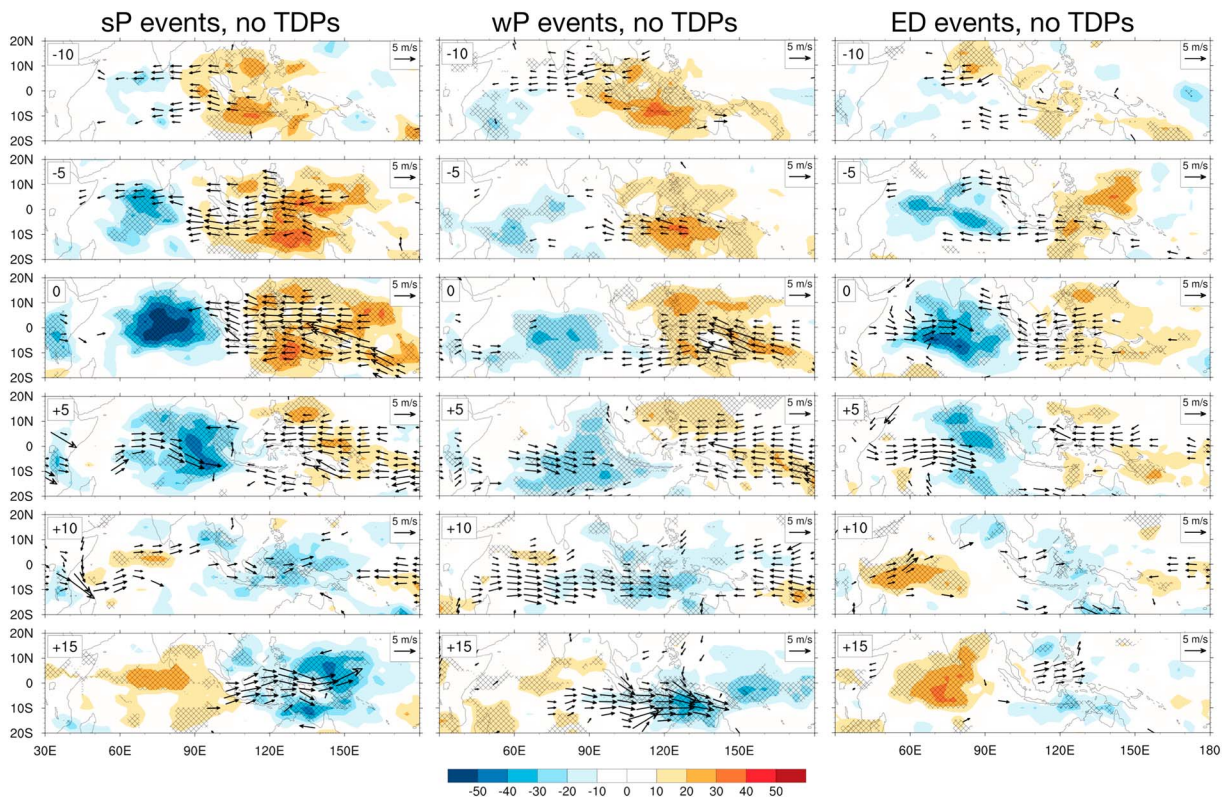
Figure 13. Composite evolution of OLR (shading) and 850-hPa winds (vectors) for sP, wP, and ED MJO events not affected by TDPs for 5-day averages listed in boxes at upper left. Hatching indicates where the mean is significantly different from zero ($p \leq 0.05$). Vectors are drawn if either zonal or meridional winds are significant using the same criteria. sP = strong propagating; wP = weak propagating; MJO = Madden-Julian oscillation; ED = eastward decaying; TDPs = transient dry precursors; OLR = outgoing longwave radiation.

since this is the level of peak moistening by zonal advection (e.g., DeMott et al., 2014). As shown in Figure 14f, the southern MC region in ED events experiences midlevel drying by two terms: the anomalous wind acting on the mean moisture gradient and the mean wind acting on the perturbation moisture gradient. Differences in the first term are driven by the weak moisture zonal gradient within and west of the southern MC region for ED events (see Figure 11), as well as weaker wind anomalies. Area- and time-averaged perturbation 850-hPa zonal winds for sP, wP, and ED for this region are −2.7, −2.0, and −1.5 m/s, respectively. The monotonic decrease in low-level easterlies from sP to ED events mirrors the reduction in dry-phase intensity and supports the idea that a strong suppressed phase contributes to moistening via winds associated with the dry ER waves driven by radiative cooling (Kim et al., 2014).

Strong drying by the mean zonal wind acting on the perturbation moisture zonal gradient also contributes to southern MC drying in ED events. In the southern MC region, the perturbation moisture zonal gradients are all negative, as Indian Ocean moist anomalies transition to western Pacific dry anomalies (Figure 13, day −5 to +5). The gradients are strongest in sP events, and weakest in ED events, but the differences are not significant (not shown). Likewise, the background midlevel winds are weak easterly in this region, but ED event easterlies are stronger than wP easterlies (−1.8 and −0.5 m/s, respectively). These differences are significant at the 90% confidence interval, but not at the 95% level, as the 95% standard error bars for wP and ED events barely overlap (not shown). Because the moisture gradient is weakest in ED events, but drying by this term is significantly stronger than in wP events, we conclude that the background wind is mostly responsible for drying by this term, although our small sample size prohibits us from stating this with more certainty.

6. Discussion

The modulation of TDP- and non-TDP-affected MJO events by La Niña and El Niño, respectively, is summarized in Figure 15 and Table 3. During La Niña conditions, the split between the ITCZ and the South Pacific
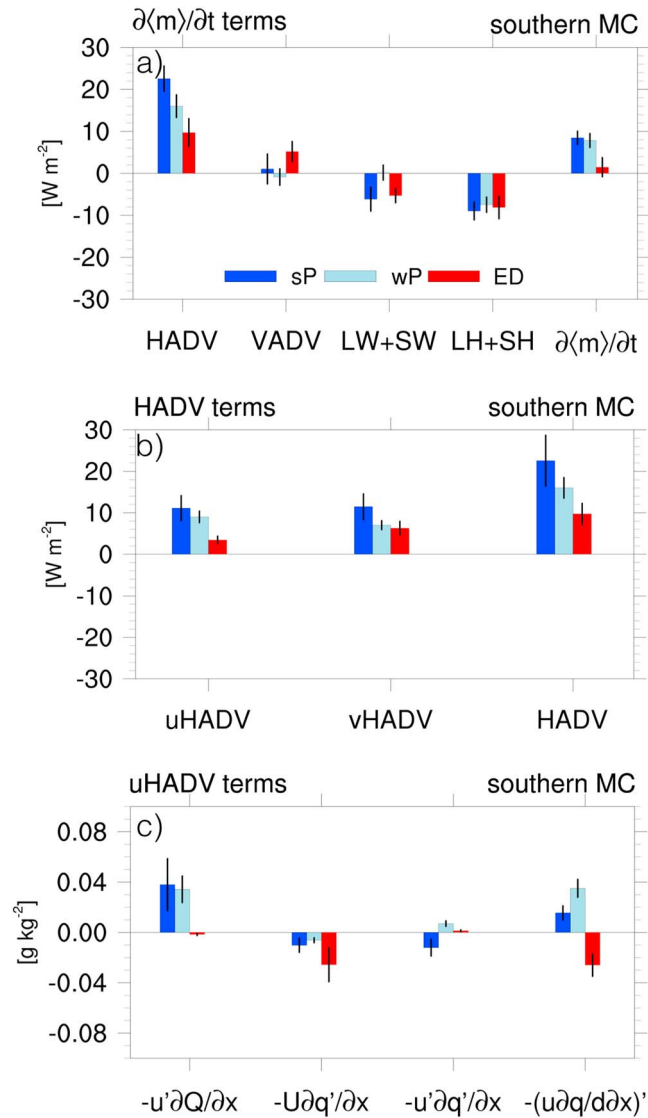
Figure 14. (a and b) MSE tendency terms and 850 to (c) 500-hPa moisture tendency terms for MJO events not affected by TDPs averaged over the southern MC box (Figure 12) and pentads centered on −5, 0, and +5 days (Figure 13) for sP (dark blue), wP (light blue), and ED (red) events. In Figure 14a, terms are described in equation (1) and section 2.1; in Figure 14b, HADV is decomposed into its zonal and meridional components ($-u\partial\langle m\rangle/\partial x$ and $-v\partial\langle m\rangle/\partial y$, respectively); and in Figure 14c, 850 to 500-hPa averaged zonal moisture advection is decomposed into components associated with anomalous (u') and background (U) zonal wind and anomalous (q') and background (Q) moisture. For a given term, differences among MJO event types are significant ($p \leq 0.05$) when thin vertical lines do not overlap. MJO = Madden-Julian oscillation; ED = eastward decaying; VADV = VADV = vertical advection; HADV = horizontal advection; MSE = moist static energy; MC = Maritime Continent; LW = longwave; SW = shortwave; LH = latent heat; SH = sensible heat.

Convergence Zone reaches into the far western Pacific (Figure 5). ER wave equatorial easterly winds (Figure 7) transport dry air from the central Pacific into the equatorial western Pacific and eastern MC where it can destructively interfere with MJO moisture anomalies. At the same time, positive precipitable water anomalies are observed over the central and western MC, which pushes meridional moisture gradients poleward (Figure 5b). Moisture mixing by ER wave meridional winds in this region is therefore also pushed poleward. Thus, during La Niña years, eastward propagating MJO convection is protected from TDPs in the eastern Indian Ocean and western MC. However, once MJO convection reaches 120°E, its moisture anomaly must be large enough to withstand mixing by TDPs near the Equator.
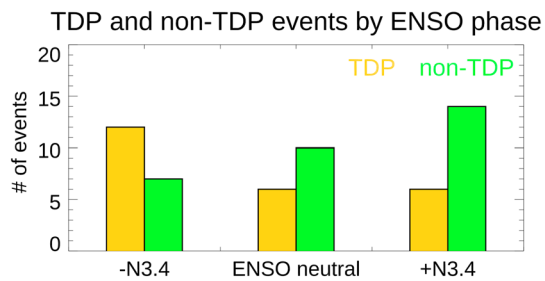
Figure 15. Frequency of TDP (orange) and non-TDP (green) MJO events as a function of ENSO state. TDP = transient dry precursor; MJO = Madden-Julian oscillation; ENSO = El Niño–Southern Oscillation.

The La Niña mean state moisture distribution that regulates moistening and drying by ER waves also influences moistening driven by MJO circulation anomalies. The sharper zonal moisture gradient in the eastern Indian Ocean and the reduced gradient in the western Pacific Ocean (Figure 9c), respectively, may have a similar effect on MJO propagation as the La Niña TDPs. That is, they would favor MJO propagation in the eastern Indian Ocean but retard it in the western Pacific Ocean. However, the sparse regions of statistically significant mean state differences in Figure 9 warrant further consideration. The limited areas of statistical significance could simply be a consequence of the small sample sizes for each MJO-type and TDP-type pairing. However, this could also result from contributions from other mechanisms that are not explicitly linked to tropical moisture distributions, such as tropical-extratropical interactions (Stan et al., 2017) or interactions with the quasi-biennial oscillation (e.g., Son et al., 2017; Yoo & Son, 2016).

During El Niño conditions, there is a reversal of moisture anomaly patterns and TDP activity, as can be inferred by flipping the signs in Figure 5. Peak moisture and its zonal gradient shift eastward. Meridional moisture gradients in the western Pacific expand poleward, while those in the eastern Indian Ocean contract equatorward. In the Indian Ocean, drying by ER wave meridional winds shifts closer to the Equator, where it is poised to interfere with MJO convection. It is possible that some of the non-TDP-affected ED events undergo drying by TDPs in the eastern Indian Ocean, which would contribute to their decay. Our TDP algorithm only selects TDPs entering the MC from the east and does not preclude equatorial TDPs that may emerge in the eastern Indian Ocean as the mean moisture contracts equatorward. ED OLR anomalies appear to "split" into two halves about the Equator on day +5 near 90°E (Figure 13), which may reflect MJO-TDP interactions in that region. This splitting behavior of non-MC-crossing MJO events is evident in some observational (e.g., Feng et al., 2015) and modeling studies (e.g., Benedict & Randall, 2011; DeMott et al., 2014; Kim & Seo, 2017), but more work is needed to understand its cause.

For MJO events that develop during El Niño conditions, propagation across the MC may first depend upon not encountering a TDP in the eastern Indian Ocean. Such well-timed events then encounter an MC that is ripe for moistening on account of the enhanced zonal moisture gradients in the western Pacific Ocean (sP and wP events) and sometimes enhanced meridional gradients over the southern MC (sP events; Figure 11c). In the southern MC region, where MJO propagation differences are largest for non-TDP-affected events, ED events are hindered by both weak moisture gradients and winds. The former might be linked to the phase of the Australian summer monsoon, while the latter is linked to the weak MJO suppressed phase.

To a first order, partitioning MJO events into those that are and are not affected by TDPs over the western MC essentially results in a composite of MJO events by ENSO phase. It is possible that ENSO regulation of the background state obscures the expression of other processes that may contribute to MJO decay, particularly those driven by MC topography, land-sea contrasts, and the robust diurnal cycle of convection.

Table 3
TDP and Non-TDP MJO Events by ENSO Phase

Event type	La Niña	Neutral	El Niño
sP, TDP	4	3	1
sP, no TDP	2	2	3
wP, TDP	3	2	3
wP, no TDP	3	5	8
ED, TDP	5	1	2
ED, no TDP	2	3	3

Note. TDP = transient dry precursor; ED = eastward decaying; MJO = Madden-Julian oscillation; ENSO = El Niño–Southern Oscillation; sP = strong propagating; wP = weak propagating.

7. Summary and Conclusions

We analyzed observed MJO events with convective signals in the Indian Ocean that either propagate across or decay over the MC. Propagating events are divided into initially strong (sP) and initially weak (wP) categories based on the magnitude of their OLR anomaly dipole (i.e., their convectively active and suppressed phases) over the Warm Pool. ED events have initial dipole anomalies similar to those of wP events.

Roughly half of all MJO events encounter intense westward propagating dry air over the eastern MC, which we refer to as a "transient dry precursor," or TDP. We present evidence that TDPs are the dry phase of ER waves. The dry anomalies are the result of ER wave gyres advecting dry subtropical air into the Tropics and advecting dry eastern Pacific air westward. TDPs originate near or east of the dateline and represent an external disruption to the MJO preconvective moistening processes. TDPs are strongly modulated by mean state moisture changes driven by ENSO cycles and are more frequent in the western Pacific Ocean and eastern MC during La Niña. The relative amplitude of the MJO moist anomaly compared to the amplitude of the TDP dry anomaly provides a rudimentary measure of how much TDP drying a given MJO event can withstand while still maintaining a positive moisture anomaly over the MC. sP and wP MJO events have surplus moisture, while ED events have a moisture deficit.

MJO events that do not encounter TDPs over the MC are more common during El Niño conditions. The eastward shift of Warm Pool precipitable water during El Niño reduces the background moisture zonal and meridional gradients that promote TDP formation. In these conditions, moistening by HADV over the southern MC appears to be the principal regulator of MJO propagation or decay, consistent with recent work by Kim et al. (2017), although the effects of tropical-subtropical interactions or MJO-quasi-biennial oscillation interactions are not ruled out. For ED events, southern MC moistening is weak because moisture gradients (zonal and meridional) and easterly wind anomalies are both weak. In contrast, the moisture gradients and winds for sP and wP events are both strong.

The purpose of separating MJO events into groups that do and do not encounter TDPs over the MC was to isolate non-TDP-affected MJO events whose decay over the MC might be linked to MC island topography, land-sea contrast, or diurnal cycle of convection. Instead, our TDP/non-TDP categories largely reflect the influence of La Niña and El Niño, respectively. While this study provides new insights into how ENSO regulates moistening and drying (via westward propagating ER waves) that can disrupt the MJO, the pervasive influence of ENSO revealed in this study may obscure the expression of MC island processes that affect the MJO. Such processes may be more evident when studying only those MJO events that develop under ENSO-neutral conditions.

References

Adames, Á. F., & Wallace, J. M. (2015). Three-dimensional structure and evolution of the moisture field in the MJO. *Journal of the Atmospheric Sciences*, *72*(10), 3733–3754.

Benedict, J. J., Pritchard, M. S., & Collins, W. D. (2015). Sensitivity of MJO propagation to a robust positive Indian Ocean dipole event in the superparameterized CAM. *Journal of Advances in Modeling Earth Systems*, *7*, 1901–1917. https://doi.org/10.1002/2015MS000530

Benedict, J. J., & Randall, D. A. (2011). Impacts of idealized air–sea coupling on Madden–Julian oscillation structure in the superparameterized CAM. *Journal of the Atmospheric Sciences*, *68*, 1990–2008.

DeMott, C. A., Benedict, J. J., Klingaman, N. P., Woolnough, S. J., & Randall, D. A. (2016). Diagnosing ocean feedbacks to the MJO: SST-modulated surface fluxes and the moist static energy budget. *Journal of Geophysical Research: Atmospheres*, *121*, 8350–8373. https://doi.org/10.1002/2016JD025098

DeMott, C. A., Klingaman, N. P., & Woolnough, S. J. (2015). Atmosphere-ocean coupled processes in the Madden–Julian oscillation. *Reviews of Geophysics*, *53*, 1099–1154. https://doi.org/10.1002/2014RG000478

DeMott, C. A., Stan, C., Randall, D. A., & Branson, M. D. (2014). Intraseasonal variability in coupled GCMs: The roles of ocean feedbacks and model physics. *Journal of Climate*, *27*(13), 4970–4995. https://doi.org/10.1175/jcli-d-13-00760.1

Dee, D. P., Uppala, S., Simmons, A., Berrisford, P., Poli, P., Kobayashi, S., et al. (2011). The ERA–Interim reanalysis: Configuration and performance of the data assimilation system. *Quarterly Journal of the Royal Meteorological Society*, *137*, 553–597.

Feng, J., Li, T., & Zhu, W. (2015). Propagating and nonpropagating MJO events over Maritime Continent. *Journal of Climate*, *28*(21), 8430–8449.

Gonzalez, A. O., & Jiang, X. (2017). Winter mean lower-tropospheric moisture over the maritime continent as a climate model diagnostic metric for the propagation of the Madden-Julian oscillation. *Geophysical Research Letters*, *44*, 2588–2596. https://doi.org/10.1002/2016GL072430

Higgins, R. W., & Mo, K. C. (1997). Persistent North Pacific circulation anomalies and the tropical intraseasonal oscillation. *Journal of Climate*, *10*(2), 223–244.

Hirata, F. E., Webster, P. J., & Toma, V. E. (2013). Distinct manifestations of austral summer tropical intraseasonal oscillations. *Geophysical Research Letters*, *40*, 3337–3341. https://doi.org/10.1002/grl.50632

Hsu, H.-H., & Lee, M.-Y. (2005). Topographic effects on the eastward propagation and initiation of the Madden-Julian oscillation. *Journal of Climate*, *18*(6), 795–809.

Hsu, P.-C., & Li, T. (2012). Role of the boundary layer moisture asymmetry in causing the eastward propagation of the Madden–Julian oscillation. *Journal of Climate*, *25*, 4914–4931.

Hung, M.-P., Lin, J.-L., Wang, W., Kim, D., Shinoda, T., & Weaver, S. J. (2013). MJO and convectively coupled equatorial waves simulated by CMIP5 climate models. *Journal of Climate*, *26*(17), 6185–6214. https://doi.org/10.1175/jcli-d-12-00541.1

Inness, P. M. M., & Slingo, J. M. M. (2006). The interaction of the Madden–Julian oscillation with the Maritime Continent in a GCM. *Quarterly Journal of the Royal Meteorological Society*, *132*(618), 1645–1667.

Jiang, X. (2017). Key processes for the eastward propagation of the Madden-Julian oscillation based on multimodel simulations. *Journal of Geophysical Research: Atmospheres*, *122*, 755–770. https://doi.org/10.1002/2016JD025955

Jiang, X., Waliser, D. E., Xavier, P. K., Petch, J., Klingaman, N. P., Woolnough, S. J., et al. (2015). Vertical structure and physical processes of the Madden–Julian oscillation: Exploring key model physics in climate simulations. *Journal of Geophysical Research: Atmospheres*, *120*, 4718–4748. https://doi.org/10.1002/2014JD022375

Kerns, B. W., & Chen, S. S. (2016). Large-scale precipitation tracking and the MJO over the Maritime Continent and Indo-Pacific warm pool. *Journal of Geophysical Research: Atmospheres*, *121*, 8755–8776. https://doi.org/10.1002/2015JD024661

Kiladis, G. N., Dias, J., Straub, K. H., Wheeler, M. C., Tulich, S. N., Weickmann, K. M., & Ventrice, M. J. (2014). A comparison of OLR and circulation–based indices for tracking the MJO. *Monthly Weather Review*, *142*, 1697–1715.

Kiladis, G. N., & Wheeler, M. (1995). Horizontal and vertical structure of observed tropospheric equatorial Rossby waves. *Journal of Geophysical Research*, *100*, 22,981–22,998. https://doi.org/10.1029/95JD02415

Kiladis, G. N., Wheeler, M. C., Haertel, P. T., Straub, K. H., & Roundy, P. E. (2009). Convectively coupled equatorial waves. *Reviews of Geophysics*, *47*, RG2003. https://doi.org/10.1029/2008RG000266

Kim, D., Kim, H., & Lee, M.-I. (2017). Why does the MJO detour the Maritime Continent during austral summer?. *Geophysical Research Letters*, *44*, 2579–2587. https://doi.org/10.1002/2017GL072643

Kim, D., Kug, J.-S., & Sobel, A. H. (2014). Propagating versus nonpropagating Madden–Julian oscillation events. *Journal of Climate*, *27*, 111–125.

Kim, G.-U., & Seo, K.-H. (2017). Identifying a key physical factor sensitive to the performance of Madden–Julian oscillation simulation in climate models. *Climate Dynamics*, *50*(1-2), 391–401.

Kiranmayi, L., & Maloney, E. D. (2011). Intraseasonal moist static energy budget in reanalysis data. *Journal of Geophysical Research*, *116*, D21117. https://doi.org/10.1029/2011JD016031

Klingaman, N. P., Woolnough, S. J., Jiang, X., Waliser, D., Petch, J., Caian, M., et al. (2015). Vertical structure and physical processes of the Madden–Julian oscillation: Linking hindcast fidelity to simulated diabatic heating and moistening. *Journal of Geophysical Research: Atmospheres*, *120*, 4671–4689. https://doi.org/10.1002/2014JD022374

Liebmann, B. (1996). Description of a complete (interpolated) outgoing longwave radiation dataset. *Bulletin of the American Meteorological Society*, *77*, 1275–1277.

Ling, J., Zhang, C., Wang, S., & Li, C. (2017). A new interpretation of the ability of global models to simulate the MJO. *Geophysical Research Letters*, *44*, 5798–5806. https://doi.org/10.1002/2017GL073891

Madden, R. A., & Julian, P. R. (1971). Detection of a 40-50 day oscillation in the zonal wind in the tropical Pacific. *Journal of the Atmospheric Sciences*, *28*, 702–708.

Madden, R. A., & Julian, P. R. (1972). Description of global-scale circulation cells in the tropics with a 40–50 day period. *Journal of the Atmospheric Sciences*, *29*, 1109–1123.

Maloney, E. D. (2009). The moist static energy budget of a composite tropical intraseasonal oscillation in a climate model. *Journal of Climate*, *22*, 711–729.

Matthews, A. J., & Meredith, M. P. (2004). Variability of Antarctic circumpolar transport and the Southern Annular Mode associated with the Madden–Julian oscillation. *Geophysical Research Letters*, *31*, L24312. https://doi.org/10.1029/2004GL021666

McPhaden, M. J., Busalacchi, A. J., Cheney, R., Donguy, J.-R., Gage, K. S., Halpern, D., et al. (1998). The Tropical Ocean-Global Atmosphere observing system: A decade of progress. *Journal of Geophysical Research*, *103*, 14,169–14,240. https://doi.org/10.1029/97JC02906

Neale, R., & Slingo, J. (2003). The Maritime Continent and its role in the global climate: A GCM study. *Journal of Climate*, *16*(5), 834–848.

Pohl, B., & Matthews, A. J. (2007). Observed changes in the lifetime and amplitude of the Madden–Julian oscillation associated with interannual ENSO sea surface temperature anomalies. *Journal of Climate*, *20*, 2659–2674.

Raymond, D. J., & Fuchs, Z. (2009). Moisture modes and the Madden-Julian oscillation. *Journal of Climate*, *22*, 3031–3046.

Roundy, P. E., & Frank, W. M. (2004). A climatology of waves in the equatorial region. *Journal of the Atmospheric Sciences*, *61*(17), 2105–2132.

Shinoda, T. (2005). Impact of diurnal cycle of solar radiation on intraseasonal SST variability in the western equatorial Pacific. *Journal of Climate*, *18*, 2628–2636.

Sobel, A. H., Maloney, E. D., Bellon, G., & Frierson, D. M. (2010). Surface fluxes and tropical intraseasonal variability: A reassessment. *Journal of Advances in Modeling Earth Systems*, *2*, 2. https://doi.org/10.3894/JAMES. 2010.2.2

Son, S.-W., Lim, Y., Yoo, C., Hendon, H. H., & Kim, J. (2017). Stratospheric control of the Madden–Julian oscillation. *Journal of Climate*, *30*(6), 1909–1922.

Stan, C., Straus, D. M., Frederiksen, J. S., Lin, H., Maloney, E. D., & Schumacher, C. (2017). Review of tropical-extratropical teleconnections on intraseasonal time scales. *Reviews of Geophysics*, *55*, 902–937. https://doi.org/10.1002/2016RG000538

Straub, K. H. (2013). MJO initiation in the real-time multivariate MJO index. *Journal of Climate*, *26*(4), 1130–1151.

Wheeler, M. C., & Hendon, H. H. (2004). An all–season real–time multivariate MJO index: Development and index for monitoring and prediction. *Monthly Weather Review*, *132*, 1917–1932.

Wilson, E. A., Gordon, A. L., & Kim, D. (2013). Observations of the Madden Julian oscillation during Indian Ocean dipole events. *Journal of Geophysical Research: Atmospheres*, *118*, 2588–2599. https://doi.org/10.1002/jgrd.50241

Woolnough, S. J., Slingo, J. M., & Hoskins, B. J. (2000). The relationship between convection and sea surface temperatures on intraseasonal timescales. *Journal of Climate*, *13*, 2086–2104.

Wu, C.-H., & Hsu, H.-H. (2009). Topographic influence on the MJO in the Maritime Continent. *Journal of Climate*, *22*(20), 5433–5448.

Yoo, C., & Son, S.-W. (2016). Modulation of the boreal wintertime Madden-Julian oscillation by the stratospheric quasi-biennial oscillation. *Geophysical Research Letters*, *43*, 1392–1398. https://doi.org/10.1002/2016GL067762

Zhang, C. (2013). Madden–Julian oscillation: Bridging weather and climate. *Bulletin of the American Meteorological Society*, *94*, 1849–1870.

Zhang, C., & Ling, J. (2017). Barrier effect of the Indo-Pacific Maritime Continent on the MJO: Perspectives from tracking MJO precipitation. *Journal of Climate*, *30*(9), 3439–3459.